

We are IntechOpen, the world's leading publisher of Open Access books Built by scientists, for scientists

6,900

Open access books available

185,000

International authors and editors

200M

Downloads

Our authors are among the

154

Countries delivered to

TOP 1%

most cited scientists

12.2%

Contributors from top 500 universities



WEB OF SCIENCE™

Selection of our books indexed in the Book Citation Index
in Web of Science™ Core Collection (BKCI)

Interested in publishing with us?
Contact book.department@intechopen.com

Numbers displayed above are based on latest data collected.
For more information visit www.intechopen.com



Fractal Structures of the Carbon Nanotube System Arrays

Raïssa S. Noule and Victor K. Kuetché

Abstract

In this work, we investigate fractals in arrays of carbon nanotubes modeled by an evolution equation derived by using a rigorous application of the reductive perturbation formalism for the Maxwell equations and for the corresponding Boltzmann kinetic equation of the distribution function of electrons in such nanomaterials. We study the integrability properties of our dynamical system by using the Weiss-Tabor-Carnevale analysis. Actually, following the leading order analysis, we write the solution in the form of series of Laurent. We also use the Kruskal's simplification to find the solutions. Using the truncated Painlevé expansion, we construct the auto-Backlund transformation of the system. We take advantage of the above properties to construct a wide panel of structures with fractals properties. As a result, we unearth some typical features, namely the fractal dromion, the fractal lump, the stochastic and nonlocal fractal excitations. We also address some physical implications of the results obtained.

Keywords: carbon nanotubes, Weiss-Tabor-Carnevale analysis, Kruskal's simplification, auto-Backlund transformation, fractal excitations

1. Introduction

Carbon nanotubes stand to be one of the wonder materials of the present century [1–3] owing to their tremendous range of physical, mechanical, thermal, electronic, and optical properties. They are found in some flat panel displays, some field-effect transistors as emerging applications exploiting the good thermal and electronic conductivities of the above nanomaterials. The carbon nanotubes were synthesized previously in 1991 as graphitic carbon needles with diameter ranging from 4 to 30 nm and length up to 1 μm [4]. Large-scale synthesis [5] provided an impetus to research in the area of carbon fiber growth, as well as in the production and characterization of fullerene materials. Two years later [6], abundant single-shell tubes with diameters of about 1 nm were synthesized. In the past few years, some studies of various nonlinear effects in carbon nanotube arrays have been achieved. There are intrinsic localized modes in strongly nonlinear systems of anharmonic lattices [7, 8], large-amplitude oscillating modes with additional features of being nonlinear as well as discrete [9], spin-wave propagation [10], propagation of short optical pulses with dispersive nonmagnetic dielectric media [11], propagation of ultimately short optical pulses in coupled graphene waveguides [12, 13].

From the reductive perturbation method, Leblond and Mihalache [14, 15] investigated the formation of ultrashort spatiotemporal optical waveforms in arrays of carbon nanotubes while deriving a new coupled system. They actually used the multiscale analysis for the Maxwell equations and for the corresponding Boltzmann kinetic equation of the distribution function of electrons. The above authors [14] showed that a perturbed few-cycle plane-wave input evolves into a robust two-dimensional light bullet propagating without being dispersed and diffracted over long distance with respect to the wavelength.

In the present work, our motivation is to investigate whether other types of robust light bullets with different features can be supported by the previous arrays. Actually, from the governing system derived by Leblond and Mihalache [14], we need to tread into its structural properties of integrability while performing the Weiss-Tabor-Carnevale approach [15] to such a problem and discuss in detail the existence of fractal solutions to the system.

Weiss, Tabor and Carnevale [15] developed one of the most powerful methods known as the Painlevé analysis [16] which is very useful in proving the integrability of a model system. Such an analysis is helpful in generating some exact solutions, no matter the model is integrable or not. Also, if ones wants only to prove the Painlevé property of a model, the use of Kruskal's simplification [17] for the WTC approach is also addressable. Thus, if we need to find some more information from the model, it is better to use the original WTC approach or some extended forms [18–21]. In this work, we combine the standard WTC approach [15] with the Kruskal's simplification [17] in view of simplifying the proof of the Painlevé integrability.

We organize the work as follows: in Section 2, we briefly present the physical background of the system under investigation. In Section 3, we perform the WTC method to the governing equations under study. Next, in Section 4, we take advantage of the arbitrary functions generated by the previous analysis to discuss some higher dimensional pattern formations of light bullets, namely the fractals. In the last section, we end with a brief conclusion.

2. Physical ground of light propagation within the carbon nanotube arrays

In a recent study, Belonenko et al. [22, 23] investigated both analytically and numerically the propagation of light bullets within an array of carbon nanotubes. They obtained an analytical function presenting some $(2 + 1)$ -dimensional optical soliton with some diffraction displays in propagation. In view of suppressing the diffraction to obtain some robust light bullet waveform, the model is slightly modified [14] while deriving a new higher dimensional coupled system. Using the calibration $\mathbf{E} = -\partial\mathbf{A}/\partial t$, \mathbf{E} and \mathbf{A} being the electric field and the potential vectors, respectively, and variable t being the time, taking into account of the dielectric and magnetic properties of carbon nanotubes [24], the Maxwell equations reduce to the following system

$$\Delta\mathbf{A} - \mathbf{A}_{tt}/c^2 = -\mu_0\mathbf{J}, \quad (1)$$

where subscripts denote the partial derivatives. Constants μ_0 and c are magnetic permeability and light velocity in vacuum, respectively. We have neglected the diffraction blooming of the laser beam in the directions perpendicular to the propagation plane. The current \mathbf{J} is directed along the axis of the nanotubes, i.e., $\mathbf{J} = J_z\mathbf{e}_z$, where unitary vector \mathbf{e}_z spans the z -axis. Besides, we consider the case where the wave field is polarized in the same direction, and $\mathbf{A} = A\mathbf{e}_z$.

In order to determine the current, we use a semiclassical approximation [25] taking into account the dispersion law from the quantum-mechanical model and the evolution of the ensemble of particles by the classical Boltzmann kinetic equation in the approximation of relaxation time. It comes

$$f_t - qA_t f_p = (F_0 - f)/\tau, \quad (2)$$

where constant q stands for the electron charge. The relaxation time τ can be assessed according to Ref. [26]. The quantity f is the distribution function of electrons in the nanotubes depending upon the time t and the momentum $p \equiv p(p_\varphi, p_z)$ of the electron. The azimuthal component p_φ reads $p_\varphi = s\Delta p_\varphi$, and the axial component p_z is merely denoted p below. It then appears that the integer s characterizes the momentum quantization transverse to the nanotube. We also mention that the function F_0 is the equilibrium value of the distribution f and is known as the Fermi-distribution function expressed as

$$F_0 = 1/[1 + \exp(E/k_B T_0)], \quad (3)$$

in which quantities k_B , T_0 , and E stand for the Boltzmann constant, the absolute temperature, and the energy in the conduction band, respectively. In account of the zigzag-type carbon nanotubes, the energy E is given by the Huckel π -electron approximation as follows

$$E = \gamma \sqrt{1 + 4 \cos(ap) \cos(\pi s/m) + 4 \cos^2(\pi s/m)}, \quad (4)$$

with $\gamma = 2.7eV$ and $a = 3b/2\hbar$ where constant $b = 0.142nm$ represents the distance between the adjacent carbon atoms. Constant m is the number of hexagons in the perimeter of a nanotube. The surface current density J_s can hence be expressed as

$$J_s = \frac{2q}{2\pi\hbar} \iint v f dp_\varphi dp, \quad (5)$$

where the velocity v reads $v = \partial E / \partial p$. The distribution function f can be written as

$$f = \sum_s \Delta p_\varphi \delta(p_\varphi - s\Delta p_\varphi) f_s(p, t), \quad (6)$$

with quantity f_s representing the longitudinal distribution function relative to the azimuthal quantum number s . The volume current density J is hence obtained as

$$J = \frac{Nq}{\pi\hbar} \sum_s \int v f_s dp, \quad (7)$$

where constant N represents the surface density of nanotubes in the xy -plane.

We use the powerful reductive perturbation method in the short-wave approximation regime [13, 28]. Assuming that the typical duration of the pulse is very small with respect to τ and the propagation length is very long with respect to the wavelength, we introduce the fast and slow variables

$$\theta = (t - x/V)/\varepsilon, \quad \xi = \varepsilon x, \quad (8)$$

in which the quantities ε and V denote the small perturbative parameter and the wave velocity, respectively. Accordingly, we address the following expansions

$$f_s = f_0 + \varepsilon f_1 + \dots, \quad A = A_0 + \varepsilon A_1 + \dots \quad (9)$$

Thus, at leading order ε^{-1} , Eq. (2) yields

$$f_{0t} - qA_{0t}f_{0p} = 0, \quad (10)$$

in which solution f_0 reads $f_0 = \varphi(p + qA_0)$ with φ being an arbitrary function. However, at large t , the wave A vanishes and f_0 goes to its equilibrium value F_0 . Thus, from Eq. (7), we write

$$J_0 = \frac{q}{\pi\hbar} \sum_s \int v(p + qA) f_0(p) dp. \quad (11)$$

Now, at leading order ε^{-2} , the Maxwell equations transform to

$$V = c. \quad (12)$$

The order ε^0 provides

$$(2/c)\partial^2 A_0 / \partial \xi \partial \theta = \mu_0 J_0, \quad (13)$$

which, with Eq. (11), stands for the governing model system.

The energy E is of the same order of magnitude as γ . Calculating $\gamma/k_B = 3.1 \times 10^4 K$ shows that E is very large with respect to room temperature. Thus, only the levels with the lowest energy are excited. Let us seek for this minimum for a given parameter s . Hence, we find that

$$E_{min} = \gamma |1 - 2|\cos(\pi s/m)|, \quad (14)$$

for $p = \pm\pi/a$ when $\cos(\pi s/m) > 0$ and for $p = 0$ when $\cos(\pi s/m) < 0$. Thus, as s varies, the minimum of E_{min} is zero, i.e., $s/m = \pm 1/3$ or $s/m = \pm 2/3$. Therefore, for $m = 6$, $s = 2$ or $s = 4$. Besides, in other nanotubes, there is a nonzero gap between valence and conduction bands. The gap is so great that the conductivity is very low. Hence, only the nanotubes where m is multiple of 3 contributes. In this sense, the expression of $E_s(p)$ reads

$$E_s = 2\gamma |\cos(ap/2)|, \quad (15)$$

for $s/m = 1/3$ and

$$E_s = 2\gamma |\sin(ap/2)|, \quad (16)$$

for $s/m = 2/3$. Calculating the velocity $v = \partial E / \partial p$, where variable p is substituted by $p - qA_0$, and considering the value at which the minimum is reached, we get

$$v = -a\gamma \operatorname{sgn}(\sin(aqA_0/2)) \cos(aqA_0/2), \quad (17)$$

where $\operatorname{sgn}(X)$ denotes the sign of X in both cases.

The current J_0 can hence be expressed as

$$J_0 = -Q \operatorname{sgn}(\sin(aqA_0/2)) \cos(aqA_0/2), \quad (18)$$

where $Q = (4Nq\gamma/\pi\hbar)\Phi(\gamma/k_B T_0)$. The function Φ reads

$$\Phi(X) = \int_{-\pi/2}^{\pi/2} dx/[1 + \exp(2X|\sin x|)]. \quad (19)$$

Inserting Eq. (18) into (13) yields the evolution equation. As a matter of illustration, we assume that $0 < aqA_0/2 < \pi$ and define A'_0 such that $aqA'_0/2 = aqA_0/2 - \pi/2$. Hence, we obtain

$$\partial^2 A'_0 / \partial \xi \partial \theta = -R \sin(aqA'_0/2), \quad (20)$$

with $R = (2Nq\gamma/\pi\epsilon_0\hbar c)\Phi(\gamma/k_B T_0)$. Assuming $|aqA_0/2| > \pi$, we can set $A''_0 = A_0 + \pi/aq$. Therefore, Eq. (20) remains. This shows that Eq. (20) is valid for any A_0 . Retaining the second transverse derivative in the wave Eq. (13), we derive the following

$$\partial^2 A'_0 / \partial \xi \partial \theta = (c/2) \partial^2 A'_0 / \partial y^2 - R \sin(aqA'_0/2), \quad (21)$$

which can be known as the two-dimensional sine-Gordon equation. Eq. (21) can be written as

$$A_T = -BC, \quad C_T = AB, \quad B_Z = C + \int^T B_{YY} dT, \quad (22)$$

provided $B = E_0/E_r$, $Z = x/L_r$, $T = (t - x/c)/t_r$, and $Y = y/w_r$, with $E_r = 2/(aqt_r)$, $L_r = -UE_r/R$, and $w_r = \sqrt{ct_r L_r}/2$. The assumption $\lim_{T \rightarrow -\infty} A = U$ is regarded. The system (22) has been investigated by means of a modified Euler scheme in Z in each substep of which the equations relative to the variable T are solved by a scheme of the same type [14]. Unlikely, we develop an analytical scheme known as the WTC formalism in view of studying the full integrability of the system above while unearthing other kinds of light bullet waveforms with compact supports.

3. Painlevé analysis

According to the standard WTC method [15], if equation Eq. (22) is Painlevé integrable, then all the possible solutions of the system can be written in the full Laurent series as follows

$$A = \sum_{k=0}^{\infty} A_k g^{k+\alpha}, \quad B = \sum_{k=0}^{\infty} B_k g^{k+\beta}, \quad C = \sum_{k=0}^{\infty} C_k g^{k+\gamma}, \quad (23)$$

with sufficient arbitrary functions among A_k , B_k , C_k , and g , where $g = g(Y, Z, T)$, $A_k = A_k(Y, Z, T)$, $B_k = B_k(Y, Z, T)$, and $C_k = C_k(Y, Z, T)$ (k being nonzero integers) are analytical functions within the neighborhood of $g = 0$. The constants α , β , and γ should all be negative integers.

The leading order analysis provides the following

$$\alpha = \gamma = -2, \quad \beta = -1 \quad (24)$$

and

$$A_0 = 2(g_Z g_T - g_Y^2), \quad B_0 = 2i\epsilon g_T, \quad C_0 = -i\epsilon A_0, \quad (25)$$

where $\epsilon = \pm 1$ and $i^2 = -1$.

In order to obtain the recursion relations to determine the functions A_k , B_k , and C_k , we substitute Eqs. (23)–(25) into (22). This leads us to the following algebraic system

$$\mathcal{M}_k \mathcal{V}_k = \mathcal{T}_k, \quad (26)$$

where \mathcal{M}_k is a square matrix, $\mathcal{V}_k = (A_k, B_k, C_k)^T$, and $\mathcal{T}_k = (\mathcal{A}_k, \mathcal{B}_k, \mathcal{C}_k)^T$ with

$$\begin{aligned} \mathcal{A}_k &= -B_{k-2, ZT} + B_{k-2, YY} \\ &\quad - (k-2) [B_{k-1, Z} g_T + B_{k-1, T} g_Z - 2B_{k-1, Y} g_Y + B_{k-1} (g_{ZT} - g_{YY})] \\ &\quad + \sum_{j=1}^{k-1} A_j B_{k-j}, \end{aligned} \quad (27)$$

and

$$\mathcal{B}_k = -A_{k-1, T} - \sum_{j=1}^{k-1} C_j B_{k-j}, \quad (28)$$

with

$$\mathcal{C}_k = -C_{k-1, T} + \sum_{j=1}^{k-1} A_j B_{k-j}, \quad (29)$$

provided $A_k = B_k = C_k = 0$ for $k < 0$. The matrix \mathcal{M}_k is given by

$$\mathcal{M}_k = \begin{pmatrix} -B_0 & k(k-3)A_0/2 & 0 \\ (k-2)g_T & C_0 & B_0 \\ -B_0 & -A_0 & (k-2)g_T \end{pmatrix}. \quad (30)$$

Thus, the determinant Δ_k of the matrix \mathcal{M}_k is given by

$$\Delta_k = -(k+1)(k-2)(k-2)(k-4)(g_Z g_T - g_Y^2)g_T^2. \quad (31)$$

If the determinant Δ_k of the coefficient matrix \mathcal{M}_k is not equal to zero, then the functions A_k , B_k , and C_k can be obtained from Eq. (26) straightforwardly as unique solutions. Nonetheless, when

$$k \in \{-1, 2, 4\}, \quad (32)$$

resonances occur.

The resonance at $k = -1$ corresponds to the singularity manifold g , which is an arbitrary function, and the case $k = 0$, which is then satisfied identically by the leading order analysis provided by Eq. (25). If the model is Painlevé integrable, we require two resonance conditions at $k = 2, 4$, which are satisfied identically such that the other four arbitrary functions among A_k , B_k , and C_k can be introduced into the general series expansion given by Eq. (23).

For $k = 1$, we can easily obtain from Eq. (26)

$$\begin{aligned} A_1 &= \frac{i\varepsilon [g_T B_{0,Z} + g_Z B_{0,T} - 2g_Y B_{0,Y} + (g_{ZT} - g_{YY}) B_0 + C_{0,T}]}{g_T}, \\ B_1 &= \frac{g_T B_{0,Z} + g_Z B_{0,T} - 2g_Y B_{0,Y} + (g_{ZT} - g_{YY}) B_0 + 2C_{0,T}}{A_0}, \\ C_1 &= -i\varepsilon A_1. \end{aligned} \quad (33)$$

On the other hand, solving the case for $k = 2$, the following resonance condition is derived

$$-B_{0,ZT} + B_{0,YY} + C_{1,T} = 0. \quad (34)$$

It is straightforward to see that the resonance condition given by Eq. (34) is satisfied identically because of Eqs. (25) and (33). Then, we have, after solving Eq. (26),

$$B_2 = \frac{C_{1,T} - A_1 B_1 - B_0 A_2}{A_0}, \quad C_2 = -i\varepsilon A_2, \quad (35)$$

where one of the quantities among A_2 and C_2 is arbitrary.

For $k = 3$, Eq. (26) gives us

$$\begin{aligned} A_3 &= \frac{i\varepsilon}{2g_T} [-B_{1,ZT} + B_{1,YY} - g_T B_{2,Z} - g_Z B_{2,T} + 2g_Y B_{2,Y}] \\ &\quad + \frac{i\varepsilon}{2g_T} [-(g_{ZT} - g_{YY}) B_2 + A_1 B_2 + A_2 B_1] \\ B_3 &= \frac{1}{2A_0} [-3B_{1,ZT} + 3B_{1,YY} - 3g_T B_{2,Z} - 3g_Z B_{2,T} + 6g_Y B_{2,Y}] \\ &\quad + \frac{1}{2A_0} [-3(g_{ZT} - g_{YY}) B_2 + 2C_{2,T} + A_1 B_2 + A_2 B_1], \\ C_3 &= -i\varepsilon A_3. \end{aligned} \quad (36)$$

Let us emphasize that $\partial_g / \partial_T \equiv g_T$, and so on.

For $k = 4$, we can obtain

$$A_4 = \frac{i\varepsilon}{6g_T} (\mathcal{A}_4 + 2C_4 - 4g_T C_4), \quad B_4 = \frac{1}{3A_0} (\mathcal{A}_4 - C_4 + 2g_T C_4), \quad (37)$$

where C_4 is an arbitrary function.

Nevertheless, let us make a remark that throughout the above study, the following relations are derived:

$$B_k - i\varepsilon C_k = 0, \quad (k = 1, 2, 3, 4). \quad (38)$$

Then, for $k = 4$, Eq. (38) verifies the resonance condition. All of the resonance conditions with four arbitrary functions are satisfied identically. Hence, the system (22) is Painlevé integrable. Its complete integrability will be established if some other essential properties such as the Bäcklund transformation (BT) and the Hirota bilinearization [27–30] are derived.

The Painlevé analysis can also be used to obtain other interesting properties [15] of the $(2 + 1)$ -dimensional coupled system above. In this work, we use the standard

truncation of the WTC expansion to obtain the BT and the Hirota bilinearization [27–30] of the system (22). By setting

$$A_{k+1} = B_k = C_{k+1} = 0, \quad \text{for } k \geq 2, \quad (39)$$

Eq. (23) with (24) becomes a standard truncated expansion

$$A = A_0/g^2 + A_1/g + A_2, \quad B = B_0/g + B_1, \quad C = C_0/g^2 + C_1/g + C_2. \quad (40)$$

After vanishing A_3 and B_3 , and using Eq. (38), we can reduce the system (36) to

$$B_{1,ZT} = A_2 B_1 + B_{1,YY}, \quad A_{2,T} = -B_1 C_2, \quad C_{2,T} = A_2 B_1. \quad (41)$$

From Eq. (41), it follows that A_2, B_1, C_2 is a solution of the system (22). Besides, the truncated expansion Eq. (40) actually stands for a BT. Generally, in order to construct a typical family of solution to Eq. (22) in a simple manner, it is useful to consider very simple expressions of A_2, B_1 , and C_2 . For convenience, we fix the original seed solution as

$$A_2 = \nu, \quad B_1 = 0, \quad C_2 = -i\varepsilon\nu, \quad (42)$$

with parameter ν being an arbitrary constant. The seed solution is actually used for constructing many other solutions. However, many other classes of solutions are obtained for other existing seed solutions. It is that property of the Painlevé approach for constructing various kinds of solutions by means of arbitrary functions that makes it potential and powerfully underlying. The solutions are given by Eq. (40) expressed in a truncated form. Many solutions are constructed in a straightforward way due to the arbitrariness of these functions, provided to solve analytically or numerically some nonlinear partial differential constraint equations.

Substituting the BT from Eq. (40) and using the Eq. (42) into Eq. (22), we derive some bilinear equations which can be decoupled as

$$\begin{aligned} D_Z D_T H \cdot F &= \nu_1 H F, & D_Y D_T H \cdot F &= -\nu_2 H F, & D_Y^2 H \cdot F &= -\nu_2 H F, \\ D_Y D_T F \cdot F &= H^2/2, & D_T^2 F \cdot F &= H^2/2, & D_Y^2 F \cdot F &= H^2/2, \end{aligned} \quad (43)$$

provided $A = D_Z + E_Y$ and $C \propto (B_Z - B_Y)$ so as to express

$$B = H/F, \quad D = \nu_1 Z - 2\partial_T \ln(F), \quad E = \nu_2 Y + 2\partial_Y \ln(F), \quad (44)$$

with $\nu = \nu_1 + \nu_2$. The symbols D_Y, D_Z , and D_T refer to the Hirota operators [29–31] with respect to the variables Y, Z , and T , respectively. According to the usual procedure, the dependent function is expanded into suitable power series of a perturbation parameter and using them in Eq. (43), we can straightforwardly construct the one-, two- and N -soliton solutions (N being an integer) to Eq. (22). Nevertheless, the investigation of these solutions will be studied in detail in a separate paper. Now, knowing the BT and the related Hirota bilinearization of Eq. (22), we can conclude that the $(2+1)$ -dimensional system above is completely integrable.

After substitution Eqs. (25) and (33) into (40), we find

$$A = \nu + \frac{(D_Y^2 - D_Z D_T)g \cdot g}{g^2}, \quad B = 2i\varepsilon \partial_T (\ln |g|), \quad C = -i\varepsilon A. \quad (45)$$

In the next section, because of the arbitrariness of some functions derived from the Painlevé analysis, we aim at focusing our interest to solutions for which the quantities A and B are expressed in the reduction form Eq. (45). In order to express some exact solutions of our initial coupled evolution system, we consider the general ansatz for the function g in the form

$$g = a_0 + a_1P + a_2Q + a_3PQ, \quad (46)$$

where the parameter $a_k (k = 0, 1, 2, 3)$ is an arbitrary constant and $P = P(Z, T)$ and $Q = Q(Y, T)$ are arbitrary functions of (Z, T) and (Y, T) , respectively.

4. Discussion of some higher dimensional solutions

With this aim, we follow the method developed by Tang and Lou [32] for generating some families of diverse pattern formations while using the arbitrary functions g expressed previously.

Let us mention that for some convenience, we rewrite the variables X , Y , and T into their lower cases. Paying particular attention to fractal pattern formations, based upon the previous works carried out on the subject, we classify the above waves according to the different expressions of the generic lower dimensional function Θ of two generalized coordinates (ξ, t) as defined by [33].

1. *Nonlocal fractal pattern*: we have the following

$$\Theta(\xi, t) = \sum_{j=1}^2 \lambda_j \theta_j |\theta_j| \left\{ \left\{ \alpha_j \sin \left[\ln \left(\theta_j^2 \right) \right] + \beta_j \cos \left[\ln \left(\theta_j^2 \right) \right] \right\} \right\}, \quad (47)$$

provided quantities θ_{0j} , λ_j , α_j , and β_j being arbitrary parameters. Also, $\theta_j \equiv k_j \xi - v_j t + \theta_{0j}$. Variables ξ , k_j , and v_j are spacelike-defined, wave number, and velocity of the j -wave component, respectively.

2. *Fractal dromion pattern*: the dromion-like (lump-like) structure is exponentially (algebraically) localized on a large scale and possesses self-similar structure near the center of the pattern. The function Θ can be expressed as

$$\Theta(\xi, t) = \exp \left\{ -|\theta| \bar{N} \left\{ r + s \sin \left[\ln \left(\theta^2 \right) \right] + w \cos \left[\ln \left(\theta^2 \right) \right] \right\} \right\}, \quad (48)$$

with $\theta_j \equiv k \xi - vt + \theta_{0j}$, θ_0 being an arbitrary parameter, and constants \bar{N} , r , w , and s are arbitrary parameters. But also we can find

$$\Theta(\xi, t) = |\theta| \left\{ \bar{\alpha} \sin \left[\ln \left(\theta^2 \right) \right] + \bar{\beta} \cos \left[\ln \left(\theta^2 \right) \right] \right\} \tilde{N} / (1 + \theta^4), \quad (49)$$

for fractal lump solution. Constants $\bar{\alpha}$, $\bar{\beta}$, and \tilde{N} are arbitrary parameters.

3. *Stochastic fractal pattern*: Such typical excitation is expressed through the differentiable Weierstrass function \wp defined as

$$\wp(\xi, t) = \sum_{j=0}^N \alpha^{-j/2} \sin \left(\beta^j \theta \right), \quad N \rightarrow \infty, \quad (50)$$

with constants α and β being arbitrary parameters. A stochastic fractal excitation can be expressed as

$$\Theta(\xi, t) = \sum_{i,j} R_i(\theta_i) R_j(\theta_j), \quad (51)$$

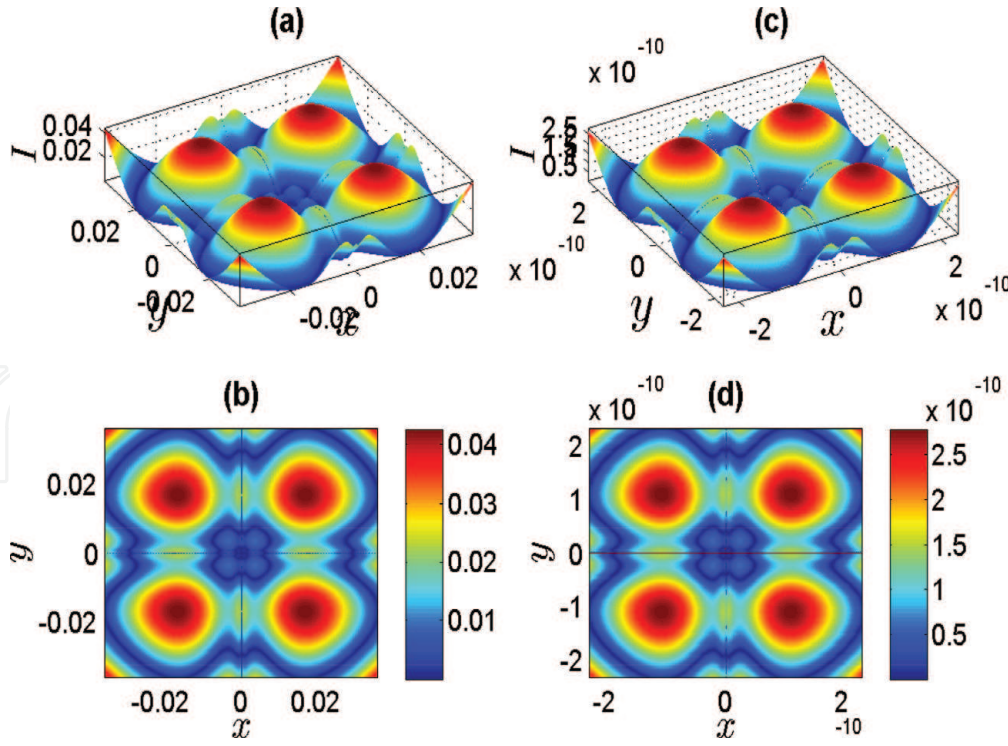


Figure 1.

Depiction of Nonlocal fractal patterns at $t = 0$. The parameters are chosen as $a_0 = 1$, $a_1 = 1$, $a_2 = 1$, and $a_3 = 1$ such that: For $p(x, t) = \Theta(x, t)$, $\lambda_1 = 1/4$, $\lambda_2 = 0$, $\theta_{01} = 0$, $k_1 = 1$, and $v_1 = 1$. For $q(y, t) = \Theta(y, t)$, $\lambda_1 = 1/4$, $\lambda_2 = 0$, $\theta_{02} = 0$, $k_2 = 1$, and $v_2 = 1$. Note that $\alpha_1 = 1$ and $\beta_1 = 0$. Panels (a) and (c) represent the pattern formations depicted in 3D-perspective, and the two others (b) and (d) are their corresponding densities represented within the square regions $[-3.6 \cdot 10^{-2}, 3.6 \cdot 10^{-2}]^2$ and $[-2.32 \cdot 10^{-10}, 2.32 \cdot 10^{-10}]^2$, respectively.

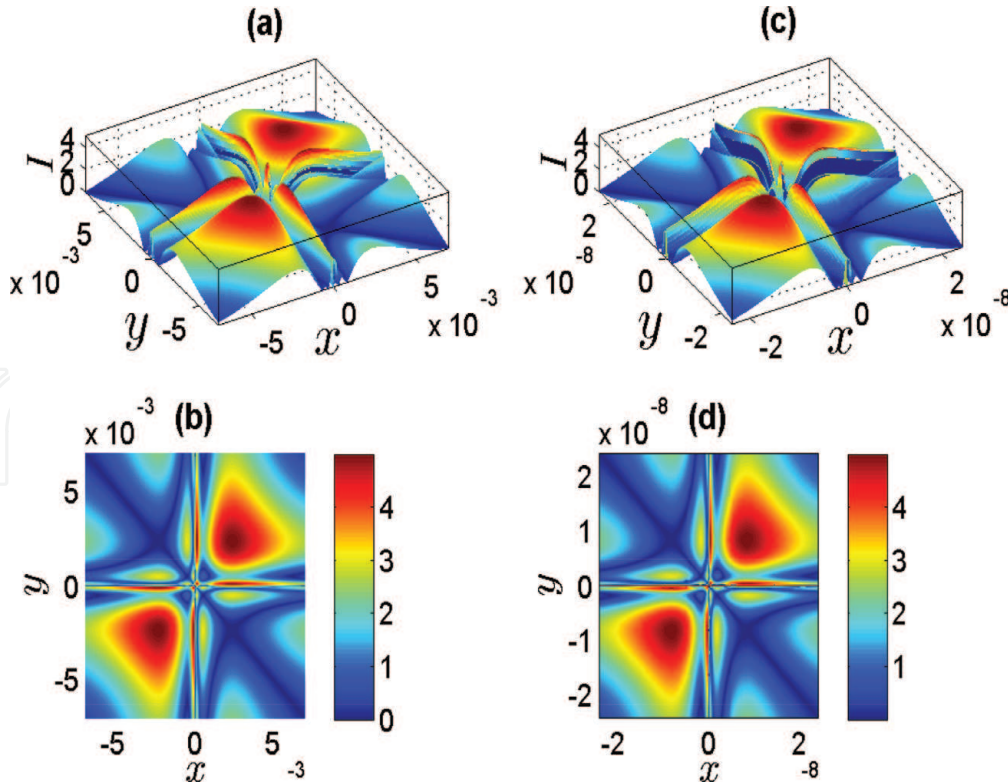


Figure 2.

Fractal dromion excitations depicted at $t = 0$ by the observable $|B| \equiv I$ which expression is given by Eq. (40). In this case, the parameters are selected as $a_0 = 1$, $a_1 = 1$, $a_2 = 1$, and $a_3 = 1$ such that: For $p(x, t) = \Theta(x, t)$, $r = 3/2$, $s = 1$, $w = 0$, $N = 1$, $\theta_{01} = 0$, $k_1 = 1$, and $v_1 = 1$. For $q(y, t) = \Theta(y, t)$, $\theta_{02} = 0$, $k_2 = 1$, and $v_2 = 1$. Panels (a) and (c) represent the pattern formations depicted in 3D-perspective, and the two others (b) and (d) are their corresponding densities represented within the square regions $[-7 \cdot 10^{-3}, 7 \cdot 10^{-3}]^2$ and $[-2.8 \cdot 10^{-8}, 2.8 \cdot 10^{-8}]^2$, respectively.

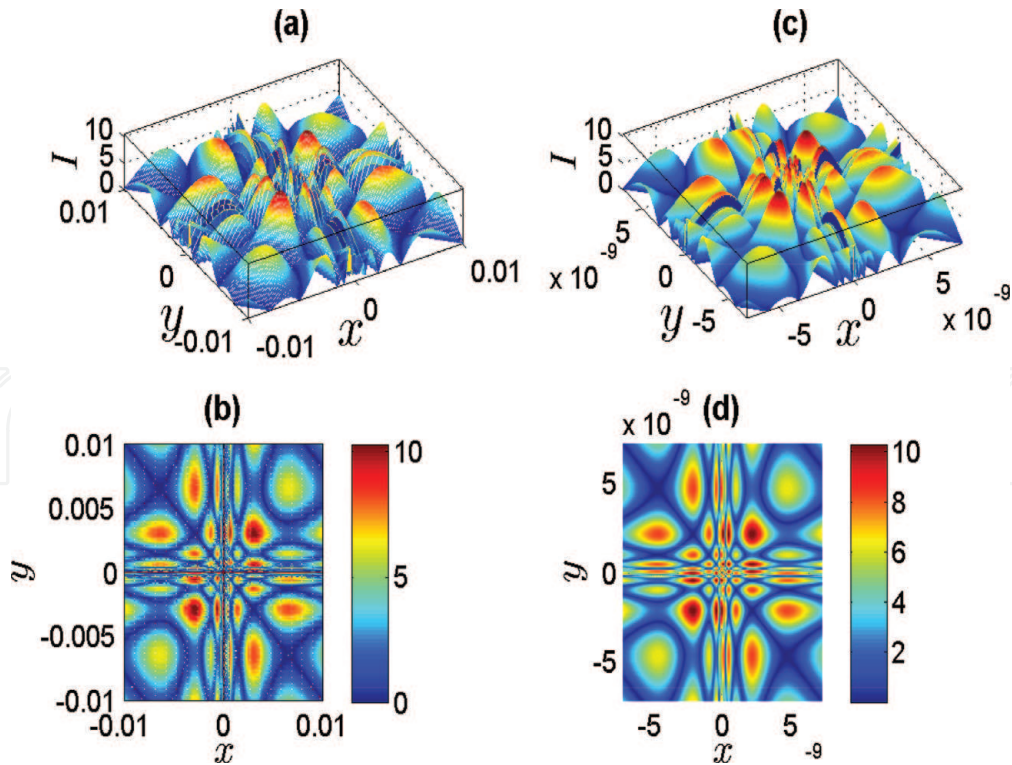


Figure 3. Fractal lump excitations depicted at $t = 0$ by the observable $|B| \equiv I$ which expression is given by Eq. (40). In this case, the parameters are selected as $a_0 = 1$, $a_1 = 1$, $a_2 = 1$, and $a_3 = 2$ such that: For $p(x, t) = \Theta(x, t)$, $\theta_{01} = 0$, $k_1 = 1$, and $v_1 = 1$. For $q(y, t) = \Theta(y, t)$, $\theta_{02} = 0$, $k_2 = 1$, and $v_2 = 1$. Note that $\bar{\alpha} = 1$, and $\bar{\beta} = 0$. Panels (a) and (c) represent the pattern formations depicted in 3D-perspective, and the two others (b) and (d) are their corresponding densities represented within the square regions $[-3.6 \cdot 10^{-2}, 3.6 \cdot 10^{-2}]^2$ and $[-2.32 \cdot 10^{-10}, 2.32 \cdot 10^{-10}]^2$, respectively.

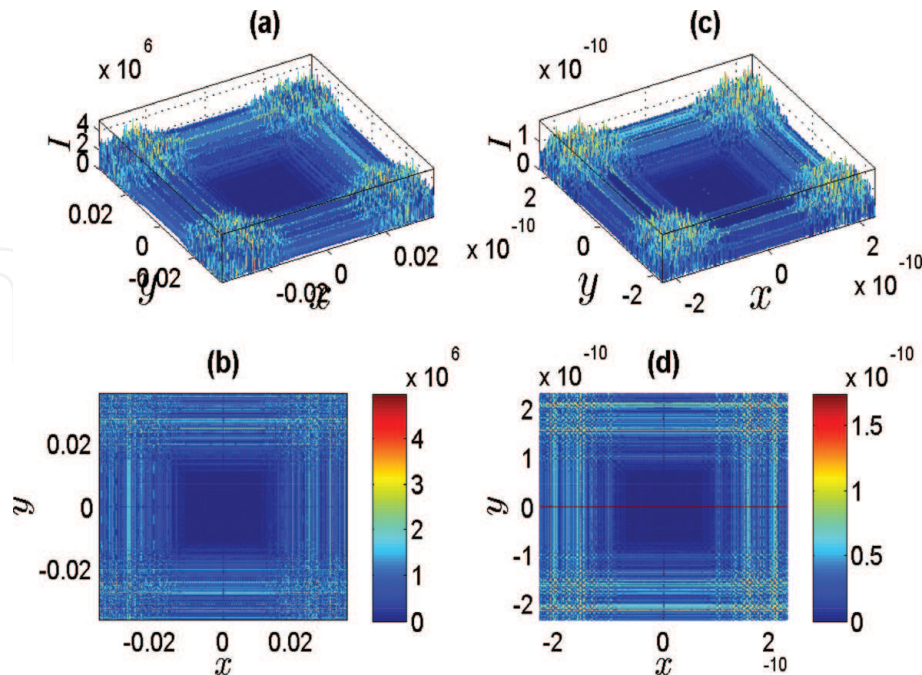


Figure 4. Fractal stochastic nonlocal excitations depicted at $t = 0$ by the observable $|B| \equiv I$ which expression is given by Eq. (40). In this case, the parameters are selected as $a_0 = 1$, $a_1 = 1$, $a_2 = 1$, and $a_3 = 1$ such that: For $p(x, t) = \Theta(x, t)$, $\lambda_1 = 1/4$, $\lambda_2 = 0$, $\theta_{01} = 0$, $k_1 = 1$, and $v_1 = 1$. For $q(y, t) = \Theta(y, t)$, $\lambda_1 = 1/4$, $\lambda_2 = 0$, $\theta_{02} = 0$, $k_2 = 1$, and $v_2 = 1$. Note that $\alpha = 3/2$, $\beta = 3/2$, and $N = 100$. Panels (a) and (c) represent the pattern formations depicted in 3D-perspective, and the two others (b) and (d) are their corresponding densities represented within the square regions $[-3.6 \cdot 10^{-2}, 3.6 \cdot 10^{-2}]^2$ and $[-2.32 \cdot 10^{-10}, 2.32 \cdot 10^{-10}]^2$, respectively.

where $R_i = \wp(\theta_i) + \theta_i^2 + \mu_i$, with μ_i standing for arbitrary parameter.

Stochastic fractal dromion/solitoff excitations: such structures are obtained by including the Weierstrass function into the dromiom solution. Especially for solitoff excitations, we can try the following:

$$\Theta(\xi, t) = k + \sum_{j=0} \eta_j \wp(\theta_j) \tanh^{\mu_j}(\theta_j), \quad (52)$$

provided quantities k , η_j , and μ_j being arbitrary parameters.

Stochastic fractal lump pattern: Eq. (51) is reduced as

$$\Theta(\xi, t) = \sum_{i,j} \rho_j R_j(\theta_j), \quad (53)$$

where quantities η_j and ρ_j being arbitrary parameter.

Now, let us analyze different figures with respect to the previous classifications. Thus, in **Figure 1**, we depict the variations of the $|\mathbf{B}|$ -observable with space at $t = 0$.

In a 3D-representation, the features presented in panel 1(a) within the space region $[-3.6 \cdot 10^{-2}, 3.6 \cdot 10^{-2}]^2 \times |\mathbf{B}|$ and those depicted in (c) within region $[-2.32 \cdot 10^{-10}, 2.32 \cdot 10^{-10}]^2 \times |\mathbf{B}|$ are self-similar nonlocal. Such a similarity in the profiles is clearly shown in panels (b) and (d) standing for their density plots, respectively.

Following the above figure, in **Figure 2**, we generate the fractal dromiom depicting self-similar structure with density plots represented in panels (b) and (d), respectively. In comparison to the previous nonlocal fractal patterns, it appears that the fractal dromions have relatively high amplitudes.

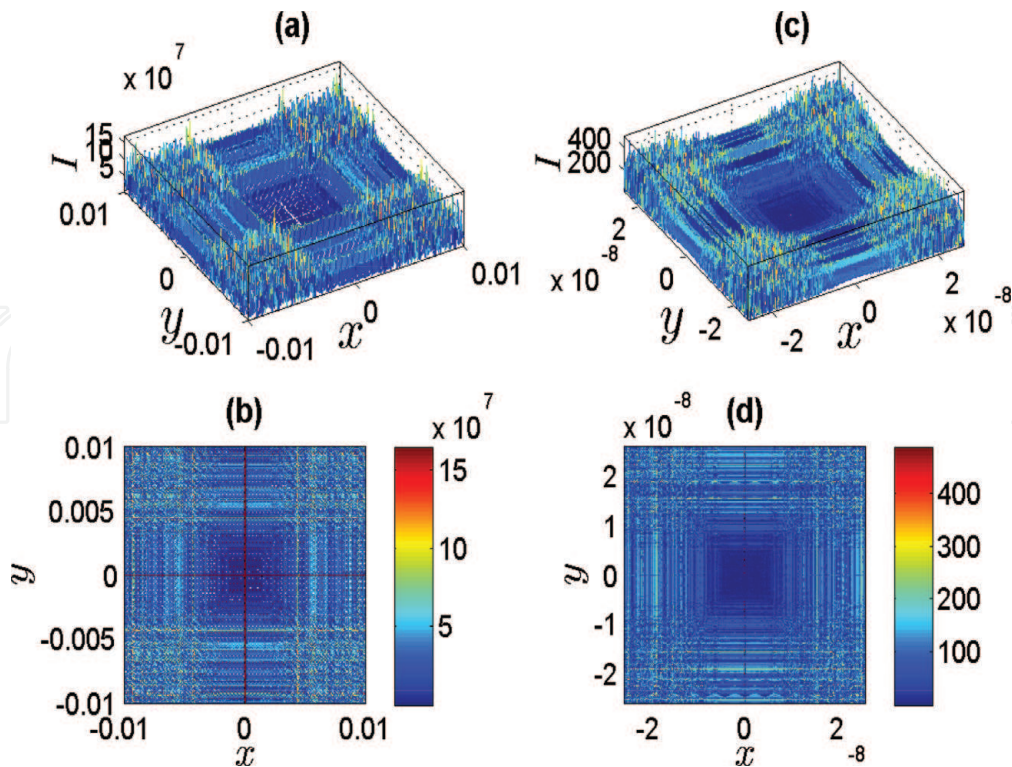


Figure 5. Fractal stochastic dromion excitations depicted at $t = 0$ by the observable $|\mathbf{B}| \equiv I$ which expression is given by Eq. (40). In this case, the parameters are selected as $a_0 = 1$, $a_1 = 1$, $a_2 = 1$, and $a_3 = 1$ such that: For $p(x, t) = \Theta(x, t)$, $r = 3/2$, $s = 1$, $w = 0$, $\overline{N} = 1$, $\theta_{01} = 0$, $k_1 = 1$, and $v_1 = 1$. For $q(y, t) = \Theta(y, t)$, $\theta_{02} = 0$, $k_2 = 1$, and $v_2 = 1$. Note that $\alpha = 3/2$, $\beta = 3/2$, and $N = 100$. Panels (a) and (c) represent the pattern formations depicted in 3D-perspective, and the two others (b) and (d) are their corresponding densities represented within the square regions $[-1 \cdot 10^{-2}, 1 \cdot 10^{-2}]^2$ and $[-2.6 \cdot 10^{-8}, 2.6 \cdot 10^{-8}]^2$, respectively.

Next, in **Figure 3**, we obtain the fractal lump which shows self-similar structures in panels (c) and (d).

In addition to the above self-similar regular fractal dromion and lump excitations, by using the lower dimensional stochastic fractal functions, we construct some other higher dimensional stochastic fractal patterns. Thus, in **Figure 4**, we generate a typical stochastic fractal nonlocal pattern with self-similarity in structure.

Besides, in **Figure 5**, with the selecting parameters and suitable choices of lower dimensional arbitrary stochastic fractal dromion function as presented in the captions of these figures, we obtain higher dimensional stochastic dromion excitations. The self-similarity in structure of the observable $I \equiv |\mathbf{B}|$ shows how the peaks are distributed stochastically within the regions $[-1 \cdot 10^{-2}, 1 \cdot 10^{-2}]^2$ and $[-2.6 \cdot 10^{-8}, 2.6 \cdot 10^{-8}]^2$ for stochastic fractal dromion.

In **Figure 6**, we construct the fractal solitoff excitations. By reducing the region $[-1.2 \cdot 10^{-2}, 1.2 \cdot 10^{-2}] \times [-5, 10]$ of panel 6(a) to $[-1.5 \cdot 10^{-8}, 1.5 \cdot 10^{-8}] \times [-5, 10]$ of panel 6(c), we obtain a totally similar structure with density plots represented in panels (b) and (d), respectively.

In **Figure 7** with the selecting parameters and suitable choices of lower dimensional arbitrary stochastic fractal lump function as presented in the captions of the figure, we obtain higher dimensional stochastic lump excitations. Through the panels (7(a) and 7(b)) depicting the variations of $|\mathbf{B}|$ —observable, at $t = 0$, the self-similarity in structure of this observable shows how the peaks are distributed stochastically within the regions $[-7 \cdot 10^{-3}, 7 \cdot 10^{-3}]^2$ and $[-2.1 \cdot 10^{-10}, 2.1 \cdot 10^{-10}]^2$. In the above configurations, the stochastic fractal solitoff

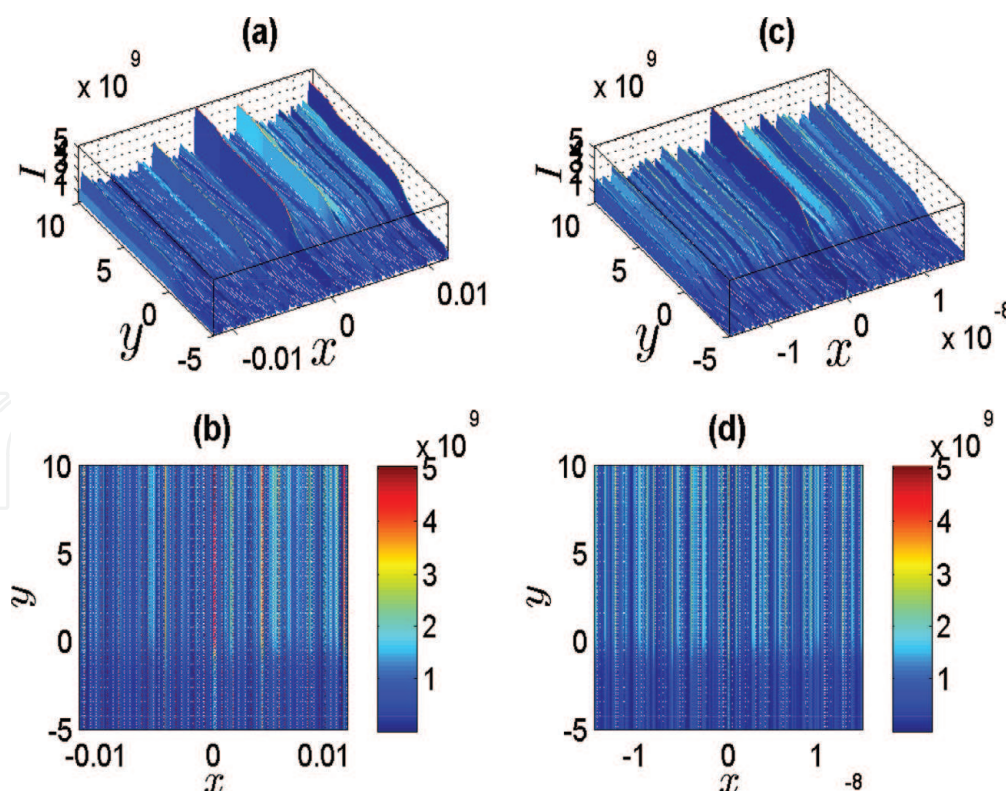


Figure 6. Fractal stochastic solitoff excitations depicted at $t = 0$ by the observable $|\mathbf{B}| \equiv I$ which expression is given by Eq. (40). In this case, the parameters are selected as $a_0 = 1$, $a_1 = 1$, $a_2 = 1$, and $a_3 = 1$ such that: For $p(x, t) = \Theta(x, t)$, $\kappa = 2$, $M = 1$, $\eta_0 = 0$, $\eta_1 = 1/2$, $\eta_m = 0 (m \geq 2)$, $\mu_1 = 1$, $\theta_{01} = -20$, $k_1 = 4$, and $v_1 = 1$. For $q(y, t) = \Theta(y, t)$, $\kappa = 0$, $M = 2$, $\eta_0 = 0$, $\eta_1 = 1/5$, $\eta_2 = 1/4$, $\eta_m = 0 (m \geq 3)$, $\mu_1 = \mu_2 = 1$, $\theta_{02} = -15$, $k_2 = 2$, and $v_2 = 2$. Note that $\alpha = 3/2$, $\beta = 3/2$, and $N = 100$. Panels (a) and (c) represent the pattern formations depicted in 3D-perspective, and the two others (b) and (d) are their corresponding densities represented within the square regions $[-1.2 \cdot 10^{-2}, 1.2 \cdot 10^{-2}] \times [-5, 10]$ and $[-1.5 \cdot 10^{-8}, 1.5 \cdot 10^{-8}] \times [-5, 10]$, respectively.

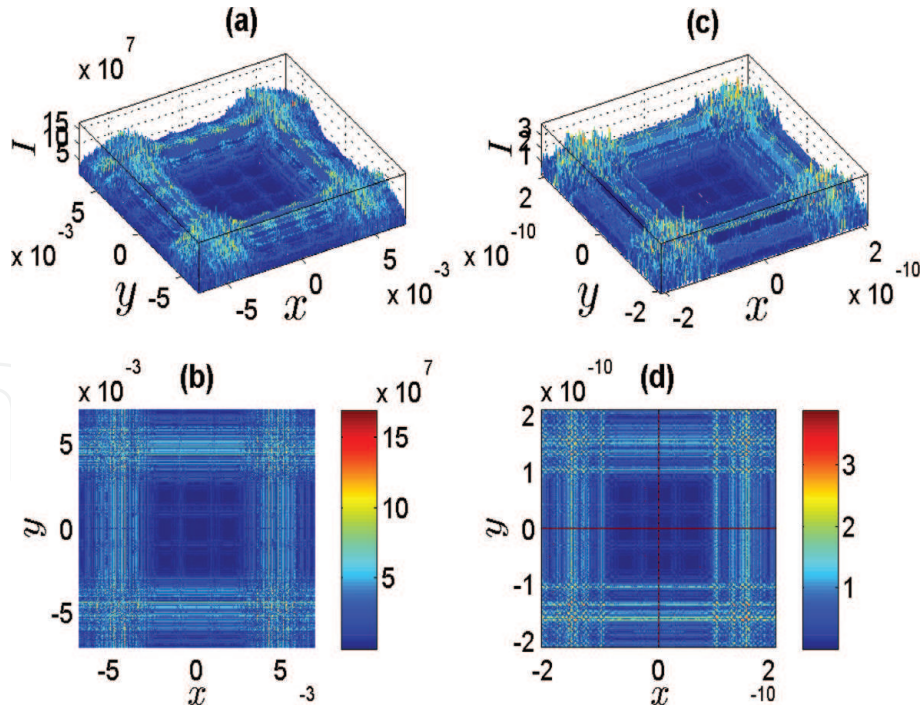


Figure 7.

Fractal stochastic lump excitations depicted at $t = 0$ by the observable $|B| \equiv I$ which expression is given by Eq. (40). In this case, the parameters are selected as $a_0 = 1$, $a_1 = 1$, $a_2 = 1$, and $a_3 = 2$ such that: For $p(x, t) = \Theta(x, t)$, $\theta_{01} = 0$, $k_1 = 1$, and $v_1 = 1$. For $q(y, t) = \Theta(y, t)$, $\theta_{02} = 0$, $k_2 = 1$, and $v_2 = 1$. Note that $\bar{\alpha} = 1$, $\bar{\beta} = 0$, $\tilde{N} = 2$ associated to $\alpha = 3/2$, $\beta = 3/2$, and $N = 100$. Panels (a) and (c) represent the pattern formations depicted in 3D-perspective, and the two others (b) and (d) are their corresponding densities represented within the square regions $[-7 \cdot 10^{-3}, 7 \cdot 10^{-3}]^2$ and $[-2.1 \cdot 10^{-10}, 2.1 \cdot 10^{-10}]^2$, respectively.

and stochastic fractal lump excitations appear to be the waves with greater amplitudes in comparison to the previous ones.

From a physical viewpoint, the observable B which has the meaning of the dimensionless electric field shows that its intensity $|B|$ can be nonlocal or rather self-confined. Actually, the intensity of the electromagnetic wave propagating along the carbon nanotube arrays is compact within the arrays. The previous study has revealed that the light bullet intensity describes a fractal-like excitation which provides more insights into the structural dynamics of the system under investigation.

5. Summary

Throughout the present work, we investigated the formation of fractal ultra-short spatiotemporal optical waveforms in arrays of carbon nanotubes. We followed the short-wave approximation to derive a generic (2+1)-dimensional coupled system. Such a coupled system was constructed via the use of the reductive perturbation analysis for the Maxwell equations and for the corresponding Boltzmann kinetic equation of the distribution function of electrons in the carbon nanotubes. Prior to the construction of different solutions to the previous coupled equations, we first studied the integrability of the governing system within the viewpoint of WTC formalism [15]. Thus, we investigated the singularity structure of the system. In this analysis, we expanded the different observables in the form of the Laurent series. Therefore, we found the leading order terms useful to solve the recurrent system. Solving this last system, we unearthed the different resonances of the governing equations. At the end, we found that the number of resonances balances seemingly the number of arbitrary functions in such a way that the governing system has sufficient and enough arbitrary functions. Hence, we derived that the

system is Painlevé integrable [15]. We derived another important properties, namely the Bäcklund transformation and the Hirota bilinearization [27–30] while establishing the complete integrability of the system.

In the wake of the result obtained from the WTC approach of integrability, we took advantage of the existence of some arbitrary functions to construct some interesting solutions such as fractals. Actually, following the investigation of fractals in many physical systems [31–33], we constructed some localized nonlinear excitations with some fractal support. As a result, we found the following typical features: the fractal dromion, the fractal lump, the stochastic and nonlocal fractal excitations.

One of the advantages of the WTC method discussed in this work is the generation of arbitrary functions useful in constructing many kinds and different solutions to the governing system. From such property endowing the method with the powerfulness, it would be rather interesting again to construct other types of nonlinear excitations such as the bubbles, the solitoffs, the dromions, the peakons, the fractals, among others [34–37]. These typical excitations would be useful in the understanding, more deeply, of the interaction between light incident excitations and carbon nanotubes for some practical issues in nanomechanical, nanoelectronic, and nanophotonic devices, alongside some emerging applications exploiting the good thermal and electronic conductivities of carbon nanotubes in some flat panel displays and field-effect transistors, among others.


Also, we intend using the WTC method in order to discover more other interesting properties still unknown in the carbon nanotube arrays. Previously, we discovered the properties of compactons in CNT [38]. The different properties will allow us in the future to improve the different uses of carbon nanotube in different areas of life. Moreover, because of these electrical and mechanical properties (very resistant, flexible, and lightweight), they are very suitable for the design of pressure sensors. These could be used by engineers to prevent structural collapses in civil engineering. They will have to measure either the pressure or the shear. Similarly, these sensors can be used in medicine while incorporating the system in textiles for better follow-up of patients or in a shoe sole. In another view, the sensors will have to be able to perform a good measure of the desired size. So to refine the design of these sensors, it will be essential to get even more information about this material. By discovering more properties of the material, we will know more how to exploit it in a safe way in all the various disciplines combining research and innovation.

Author details

Raïssa S. Noule and Victor K. Kuetché*
National Advanced School of Engineering, University of Yaounde I, Cameroon

*Address all correspondence to: vkuetche@yahoo.fr

IntechOpen

© 2019 The Author(s). Licensee IntechOpen. This chapter is distributed under the terms of the Creative Commons Attribution License (<http://creativecommons.org/licenses/by/3.0>), which permits unrestricted use, distribution, and reproduction in any medium, provided the original work is properly cited. 

References

- [1] Saito R, Dresselhaus G, Dresselhaus MS. Physical Properties of Carbon Nanotubes. London: Imperial College Press; 1998
- [2] Dresselhaus S, Dresselhaus G, Eklund PC. Science of Fullerenes and Carbon Nanotubes. New York: Academic; 1996
- [3] Charlier J-C, Blase X, Roche S. Reviews of Modern Physics. 2007;**79**:677
- [4] Iijima S. Nature (London). 1991;**354**:56
- [5] Ebbesen TW, Ajayan PM. Nature (London). 1992;**358**:220
- [6] Iijima S, Ichihashi T. Nature (London). 1993;**363**:603
- [7] Flach S, Willis CR. Physics Reports. 1998;**295**:182
- [8] Campbell DK, Flach S, Kivshar YS. Physics Today. 2004;**57**:43
- [9] Savin AV, Kivshar YS. Europhysics Letters. 2008;**82**:66002
- [10] Leblond H, Veerakumar V. Physical Review B. 2004;**70**:134413
- [11] Yanyushkina NN, Belonenko MB, Lebedev NG. Optika i Spektroskopiya. 2011;**111**:92 [Optics and Spectroscopy. 2011;**111**:85]
- [12] Belonenko MV, Lebedev NG, Yanyushkina NN. Fizika Tverdogo Tela. 2012;**54**:162 [Physics of the Solid State. 2012;**54**:174]
- [13] Harris P. Carbon Nanotubes and Related Structures. New Materials for the Twenty-First Century. New York: Cambridge University; 1999 and Moscow: Tekhnosfera; 2003
- [14] Leblond H, Mihalache D. Physical Review A. 2012;**86**:043832
- [15] Weiss J, Tabor M, Carnevale G. Journal of Mathematical Physics. 1983; **24**:522
- [16] Ramani A, Grammaticos B, Bountis T. Physics Reports. 1989;**180**:159
- [17] Jimbo M, Kruskal MD, Miwa T. Physics Letters A. 1982;**92**:59
- [18] Fordy AP, Pickering A. Physics Letters A. 1991;**160**:347
- [19] Conte R. Physics Letters A. 1989; **140**:383
- [20] Lou S-y. Physical Review Letters. 1998;**80**:5027
- [21] Lou S-y. Zeitschrift für Naturforschung. 1998;**53a**:251
- [22] Belonenko MB, Demushkina EV, Lebedev NG. Journal of Russian Laser Research. 2006;**27**:457
- [23] Belonenko MB, Lebedev NG, Popov AS. Pis'ma Zhurnal Eksperimental'noi i Teoreticheskoi Fiziki. 2010;**91**:506 [JETP Letters. 2010;**91**:461]
- [24] Landau LD, Lifshitz EM. Field Theory [in Russian]. Moscow: Fizmatlit; 1988
- [25] Landau LD, Lifshitz EM. Physical Kinetics [in Russian]. Moscow: Nauka; 1979
- [26] Tans SJ, Devoret MH, Dai H, et al. Nature. 1997;**386**:474
- [27] Manna MA, Merle V. Physical Review E. 1998;**57**:6206
- [28] Hirota R. Direct Method in Soliton Theory. Cambridge, UK: Cambridge University Press; 2004
- [29] Hirota R. Physical Review Letters. 1971;**27**:1192

[30] Hirota R, Satsuma J. Journal of the Physical Society of Japan. 1980;**40**:611

[31] Tang XY, Lou SY. Journal of Mathematical Physics. 2003;**44**:4000

[32] Kuetché VK, Bouetou TB, Kofane TC. Dynamics of miscellaneous fractal structures in higher-dimensional evolution model systems. In: Classification and Application of Fractals. New York: Nova Science Publishers; 2011

[33] Lou SY. Journal of Physics A: Mathematical and General. 2002;**35**:10619

[34] Victor KK, Thomas BB, Kofane TC. Physical Review E. 2009;**79**:056605

[35] Kuetché VK, Bouetou TB, Kofane TC, Moubissi AB, Porsezian K. Physical Review E. 2010;**82**:053619

[36] Thomas BB, Victor KK, Crepin KT. Journal of Physics A: Mathematical and Theoretical. 2008;**41**:135208

[37] Kuetché VK, Bouetou TB, Kofane TC. Journal of Mathematical Physics. 2011;**52**:092903

[38] Noule RS, Kuetché VK. Compactons in carbon nanotube arrays. In: Advances in Nonlinear Dynamics Research. New-York: Nova Science Publishers; 2016